Local helioseismology and correlation tracking analysis of surface structures in realistic simulations of solar convection

Dali Georgobiani, Junwei Zhao, Alexander G. Kosovichev

Hansen Experimental Physics Laboratory, Stanford University, Stanford, CA, 94305

David Benson, Robert F. Stein

Physics and Astronomy Department, Michigan State University, East Lansing, MI 48824

Åke Nordlund

Niels Bohr Institute, Copenhagen University, Juliane Maries Vej 30, DK–2100 København Ø, Denmark

ABSTRACT

We apply time-distance helioseismology, local correlation tracking and Fourier spatial-temporal filtering methods to realistic supergranule scale simulations of solar convection and compare the results with high-resolution observations from the SOHO Michelson Doppler Imager (MDI). Our objective is to investigate the surface and sub-surface convective structures and test helioseismic measurements. The size and grid of the computational domain are sufficient to resolve various convective scales from granulation to supergranulation. The spatial velocity spectrum is approximately a power law for scales larger than granules, with a continuous decrease in velocity amplitude with increasing size. Aside from granulation no special scales exist, although a small enhancement in power at supergranulation scales can be seen. We calculate the time-distance diagram for f- and p-modes and show that it is consistent with the SOHO/MDI observations. From the simulation data we calculate travel time maps for surface gravity waves (f-mode). We also apply correlation tracking to the simulated vertical velocity in the photosphere to calculate the corresponding horizontal flows. We compare both of these to the actual large-scale (filtered) simulation velocities. All three methods reveal similar large scale convective patterns and provide an initial test of time-distance methods.

Subject headings: convection—Sun: oscillations—methods: numerical

1. Introduction

Local helioseismology uses the observed oscillation modes to probe the near surface structure of the Sun to determine sound speed, flow velocities and magnetic field structures. One of several methods used in this field is called the time-distance helioseismology. It measures the time taken by a wave packet to travel from one point on the solar surface to another (Duvall et al. 1993; Kosovichev & Duvall 1997). The travel time for a wave depends on the wave speed and the flow velocities along the ray paths. These effects can be separated by measuring the wave travel time for waves propagating in opposite directions along the same ray paths. Inversion methods applied to infer the properties of subsurface convection and structures are based on various approximations, such as a geometric acoustic ray approximation (Kosovichev et al. 2000; Zhao et al. 2001), Fresnel-zone approximation (Jensen et al. 2001; Couvidat et al. 2004) and Born-approximation (Gizon & Birch 2002). Unfortunately, until now, there has been no direct verification of these methods (Jensen et al. 2003; Werne et al. 2004).

Realistic 3D simulations of solar convection (Stein & Nordlund 2000; Benson et al. 2006) provide a way to evaluate the accuracy and consistency of time-distance and other local helioseismology techniques. These simulations provide a realistic model of convective motions in the upper convection zone and possesses a rich spectrum of f- and p-mode oscillations excited by the turbulent convection. They can be used for testing helioseismology methods. Therefore, it is very important to apply some of the existing local helioseismology methods to the simulated solar convection, and check whether the results are consistent with the subsurface data obtained directly from the simulated flows. In addition, the comparison of the oscillation properties obtained from the numerical model, such as the velocity spectrum, $k - \omega$ diagram and time-distance (cross-covariance) diagram, with observations provides validation for the simulation model.

Previously, the realistic simulations of solar convection have been used to study the excitation mechanism of solar and stellar oscillations (Stein et al. 2004), and some properties of oscillation modes, such as the line asymmetry (Georgobiani et al. 2000). However, these simulations were carried out for small, granulation-size, computational domains. Recently, with the progress of parallel supercomputing it became possible to substantially expand the computational domain, both horizontally and in depth, and to simulate the multi-scale solar convection, from granulation to supergranular scales (Benson et al. 2006). These simulations allow us for the first time to investigate the properties of large-scale convection by applying helioseismology and other methods used to analyze solar observations, and thus test these methods and also evaluate how close the realistic simulations are to the real Sun. Such tests are particularly important for the local helioseismology methods, which are based on

simplified models of wave propagation.

The goal of this paper is to investigate the basic helioseismic properties of the large-scale 3D simulations (the oscillation power spectrum and wave travel times) and compare these with the high-resolution observations from SOHO/MDI (Scherrer et al. 1995). An initial time-distance analysis is carried out for surface gravity waves (f-mode), which are well suited for studying the surface and sub-surface structure of solar convection on supergranulation scales (Duvall & Gizon 2000). Our analysis shows that travel times from the simulation agree very well with travel times from the SOHO/MDI observations. This demonstrates that the simulated data are sufficiently close to the observed solar data, providing ground for further detailed helioseismic measurements and inversions. Large-scale structures can be detected in the simulated data set using f-mode time-distance and local correlation tracking techniques and are observed directly in filtered flow fields.

2. Numerical Model and Observed Data

We study the results of a 3D, compressible, radiative-hydrodynamic (RHD) code simulating the upper solar convection zone and photosphere. The code calculates LTE, non-gray radiation transfer and employs a realistic equation of state and opacities. More description of the code is found in Stein & Nordlund (2000); Benson et al. (2006).

The computational domain of our simulations spans 48 Mm $\times$ 48 Mm horizontally and 20 Mm vertically, with a horizontal resolution of 100 km and vertical resolution of 12 to 75 km. The three velocity components measured at 200 km above $\tau_{\rm cont} = 1$ are saved every minute. Their spatial grid is 500 by 500 pixels. The domain is sufficiently large, and the time sequence of several hours is long enough to obtain sufficient signal/noise by temporal averaging to perform a helioseismic time-distance analysis and seek evidence for the presence of large-scale flows. Eventually, the depth dependence and dynamics of these large-scale flows will be studied as well. We compare some of our findings with results obtained from SOHO/MDI high resolution observations. This observational data set is an 8.5 hour time series, with 1 minute cadence, of a 211.5 Mm $\times$ 211.5 Mm horizontal patch of the MDI Doppler velocity, on the spatial grid of 512 by 512 pixels with the resolution of about 400 km per pixel. The solar rotation is removed. Both sets of data are processed identically, whenever a comparison between the observations and simulations occurs.

3. Surface Structures

Oscillation modes in the simulations are excited naturally, due to convective motions and realistic cooling on the simulated solar surface (Georgobiani et al. 2000; Stein & Nordlund 2001; Stein et al. 2004). We use the vertical velocity component from the simulation data as a proxy for the observed Doppler velocity, and calculate the power spectrum, $P(k, \omega)$, in the horizontal wavenumber-frequency domain. Following the helioseismology convention, we represent the power spectrum in terms of the spherical harmonic degree, $\ell = kR_\odot$, where $R_\odot$ is the solar radius, and the cyclic frequency, $\nu = \omega/2\pi$.

The power spectrum ($\ell - \nu$ diagram) calculated from the simulated vertical velocity clearly shows a resolved f-mode along with a p-mode spectrum that looks very similar to the results from the SOHO/MDI Doppler images (Fig. 1). These simulations possess a richer mode spectrum than in our smaller (6 Mm wide by 3 Mm deep) simulations because the wider and deeper domain encompasses many more resonant modes within it. The spectral resolution achieved in these simulations allows us to test time-distance helioseismology measurements (Duvall et al. 1993, 1997).

Mode filtering is an essential part of the time-distance technique. The convection signals (broad wedge in the lower right part of the $\ell - \nu$ diagram) need to be removed. We construct the time-distance diagram for both simulated and observed data by computing cross-covariance of oscillation signals separated by a certain distance (Fig. 2) (Duvall et al. 1997), and find a remarkable similarity between them. Because of the higher resolution, in the numerical simulation the cross-covariance signal extends to much shorter distances than in the MDI data. This illustrates a potential for small-scale helioseismic diagnostics of observations of higher than MDI resolution, such as anticipated from the Solar-B mission (Sekii 2004).

We show in section 3.2 that the travel times from simulation data agree with travel times from the SOHO/MDI observations very well. Both the $\ell - \nu$ and time-distance diagrams illustrate the potential of the simulations for testing helioseismology measurement and inversions procedures.

In the following sections, we explore the surface structures in the simulated data, directly by averaging the flow field and using spectral analysis (Sect. 3.1), and also by implementing the f-mode time-distance analysis (Sect. 3.2), and local correlation tracking technique (Sect. 3.3).

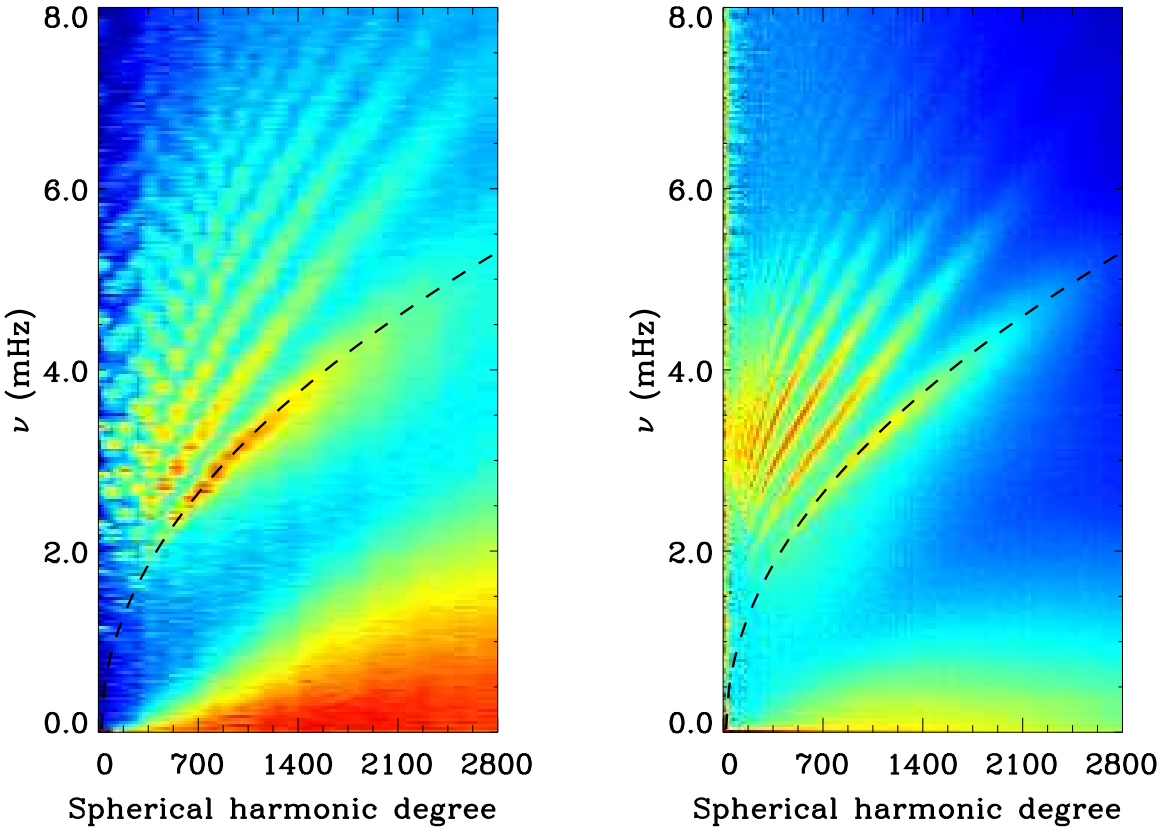

Fig. 1.— The power spectra ($\ell - \nu$ diagrams) for the simulated vertical velocity (left) and the Doppler velocity from the MDI high-resolution observations (right). The dark curve represents the theoretical f-mode.

3.1. Fourier Analysis of Surface Velocities

We analyze the simulated velocity fields by calculating spatial power spectra for both vertical and horizontal velocity components and compare these with the spatial power spectrum for the MDI Doppler signal. Power spectra are calculated for each time and are then averaged over time. This reduces the statistical fluctuations that are present in spectra from a single time. In Fig. 3 we show $V(\ell) = (\ell\, P(\ell))^{1/2}$, where $V(\ell)$ is velocity amplitude in the Fourier domain at spherical harmonic degree ℓ and $P(\ell)$ is time averaged power (velocity squared) per unit ℓ. There is a continuous decrease in the velocity amplitude from granules to larger scales. Aside from granulation no special scales are revealed in the spectra, although there may be a small enhancement in the horizontal velocity ($V_{\rm horiz}$) spectrum at

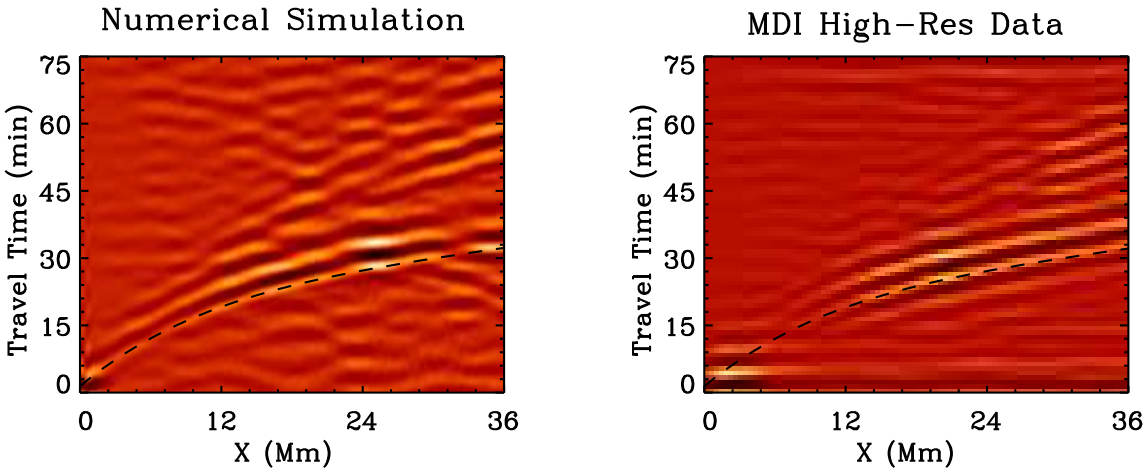

Fig. 2.— Time-distance diagrams for the simulated vertical velocity (left) and the Doppler velocity from the high-resolution MDI observations (right). The dark curve is time-distance relation computed from a standard solar model. The second bounce can be seen in both pictures.

supergranulation scales ($\ell \sim 200$).

In Fig. 4 we separate motions into 'convective' and 'oscillatory' parts, according to whether the power in Fourier space lies above or below the line $\omega = ck$, where $c = 6$ km s^{-1} is approximately equal to the sound speed of the photosphere. As illustrated by Fig. 1 this provides a rather clean split; the corresponding line in Fig. 1 would intersect the right hand side ν-axis at $\nu \approx 3.8$ mHz.

As shown by Fig. 4, the horizontal velocities at the height of the MDI Ni λ 676.78 nm line formation (about 200 km above $\tau_{500} = 1$) are almost exclusively of convective origin. The vertical velocities, on the other hand, are a mixture of convective and oscillation motions where the convective motions are dominant at smaller scales and the oscillatory motions are dominant at larger scales.

For granular and larger scales the horizontal velocities are larger than the vertical velocities and become increasingly dominant as the scale increases. The reason that large scale horizontal motions are present at these heights is that the atmosphere is not far from

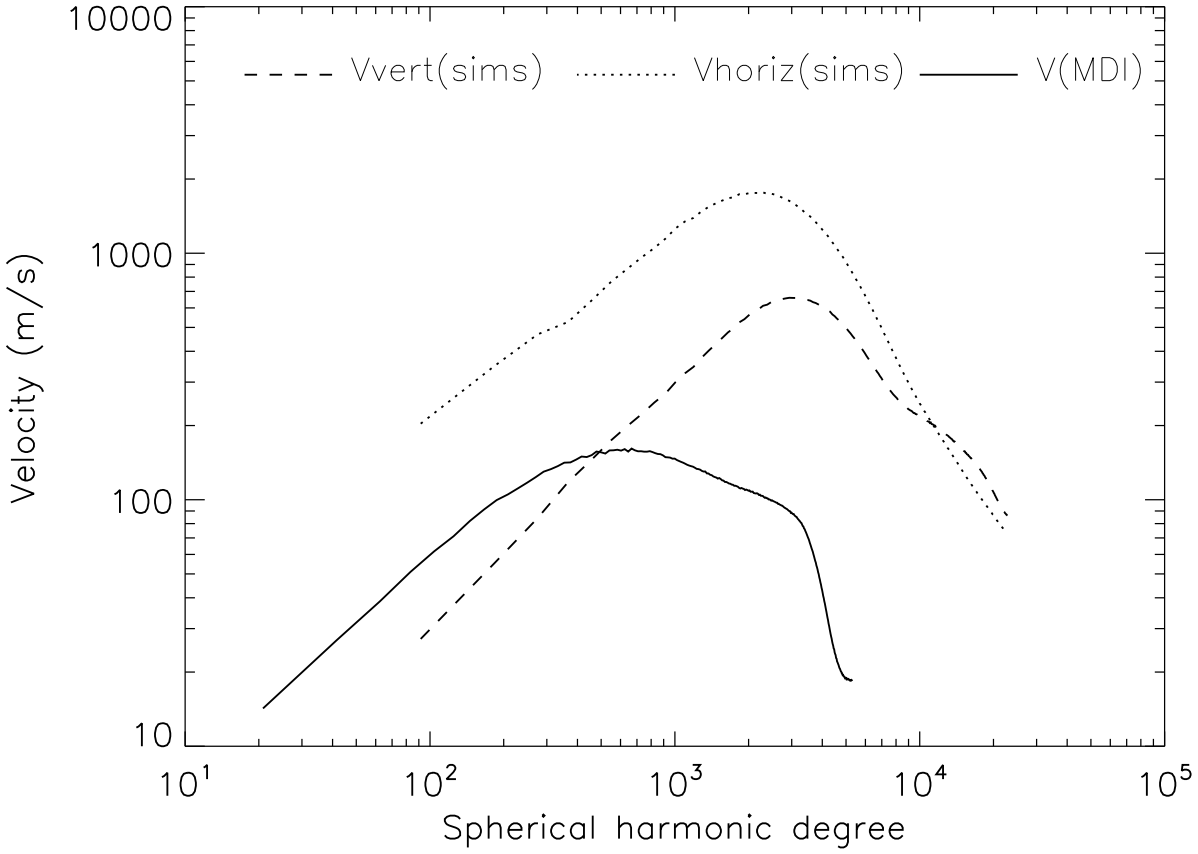

Fig. 3.— Spatial spectra for horizontal and vertical components of the simulated velocity, and the MDI Doppler signal. Spectra are calculated for individual snapshots and then time-averaged, the simulation data over 20 hours and the MDI data over 8.5 hours.

hydrostatic equilibrium and the pressure fluctuations that exist below the surface to drive the large scale horizontal flows imprint their fluctuations on the surface and produce smaller amplitude large scale horizontal flows there also (Nordlund 1982).

Because of mass conservation, vertical convective velocities decrease more rapidly with size than the horizontal ones, with the ratio of vertical to horizontal velocity amplitudes approximately inversely proportional to size (cf. the green and blue dashed lines in Fig. 4). At granular scales, where the vertical velocity peaks, the vertical convective velocity at the height of formation of the λ 676.78 nm line is still about 3–4 times weaker than the horizontal one.

In general, the MDI Doppler signal is a mix of horizontal and vertical velocities. There is

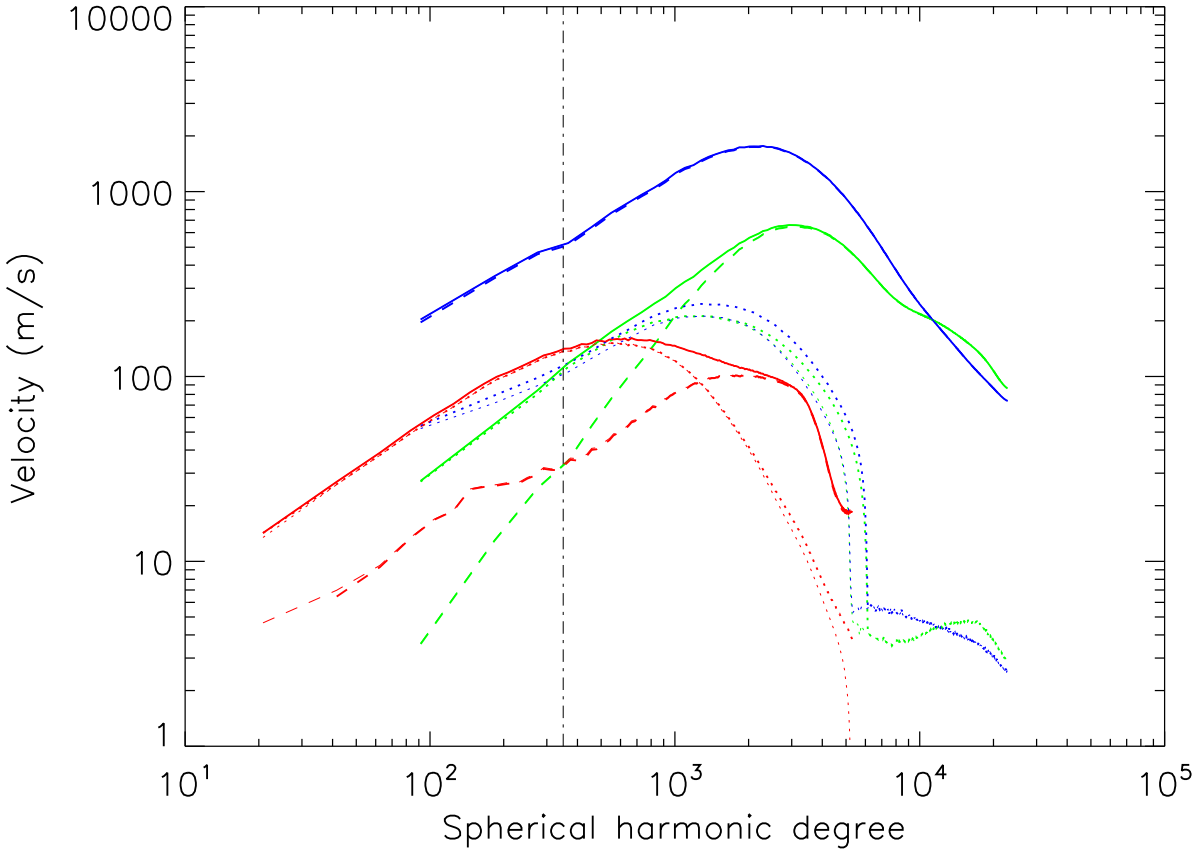

Fig. 4.— Velocity spectra separated into convective, oscillatory and total components. The oscillatory signal is negligible in the horizontal velocity but dominates the vertical velocity and MDI Doppler velocity on large scales ($\ell \leq 1000$).

no obvious way to decouple these components, although, depending on where on the solar disc the data patch was located, one can estimate the approximate contribution of the horizontal and vertical components. The current dataset was taken near solar disk center (which at the time was about 7.5 heliographic degrees below the solar equator). Nevertheless, because of the significant extension of the patch, the root-mean-square projection of horizontal velocities into the line-of-sight was about 15%, while almost 99% of the vertical velocity is projected onto the line-of-sight. Indeed, if we combine 15% of the simulated horizontal velocities and 99% of the simulated vertical velocities, multiply by the instrument Modulation Transfer Function (MTF) (Woodard et al. 2001) and compare the resulting power spectrum with the MDI power spectrum in Fig. 5, we get a good correspondence, although the simulated power at large scales (mostly oscillatory according to Fig. 4) falls somewhat short of the observed

power. Given that the numerical resolution (96 km) is somewhat marginal on granular scales, where solar oscillations are excited (Stein & Nordlund 2001), this is not surprising.

From the slope of the red dashed curve in Fig. 4 one surmises that the convective LOS velocity observed with MDI over this patch actually derives most of its contribution at large scales from the horizontal velocity field. An enhancement at supergranular scales is visible.

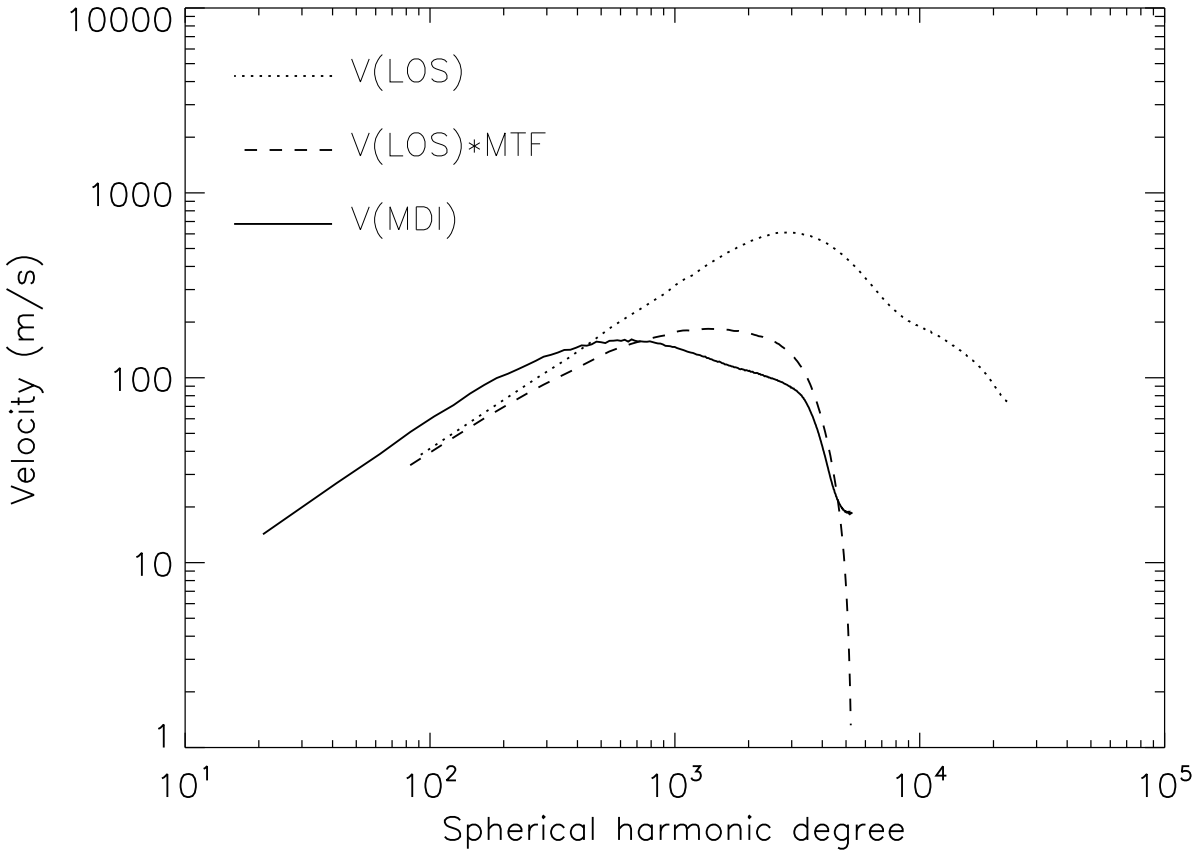

Fig. 5.— Simulated line-of-sight (LOS) component of the surface velocity spectrum (dotted), convolved with the instrumental MTF (dashed), compared with the MDI high-resolution spectrum (solid).

Averaging the velocity fields over several hours eliminates the oscillations and suppresses the small scale features but does not eliminate them. To remove the small spatial scales, it is necessary, in addition, to apply a low-pass k-space filter. We use this procedure to reveal the large-scale patterns in both vertical and horizontal velocity components. Fig. 6 (left panel) is an example of such a pattern in the V_z component. An alternative procedure would be to

filter entirely in Fourier space, eliminating the oscillations by removing power for $\omega \geq ck$ (as discussed in connection with Fig. 4 above) and then applying a low-pass filter in k.

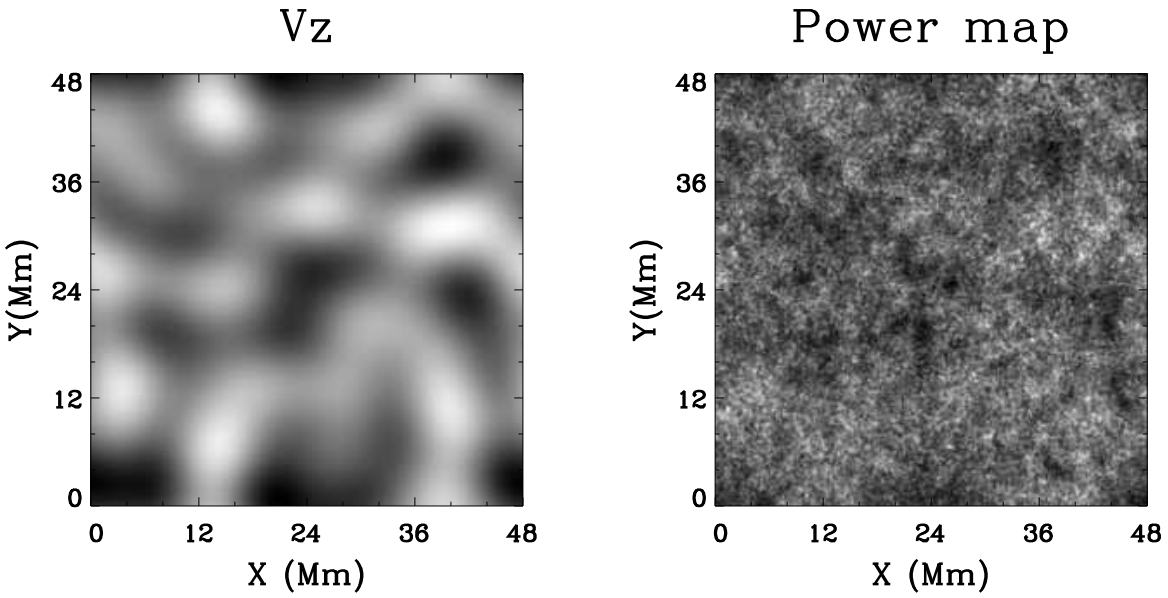

Fig. 6.— Left: Simulated large scale vertical velocity. The velocity is averaged over 8.5 hours and smoothed with a low-pass filter. Light is downflow and dark upflow. Right: p-mode power in the frequency interval 2-5 mHz. No low-pass filter has been applied. The oscillatory power is concentrated in the intergranular lanes and is weakest in the upflow centers of the large-scale structures.

We also construct p-mode power maps by Fourier-transforming the vertical velocity fields in time at each spatial point, and summing the result over the frequency interval 2-5 mHz (Fig. 6, right panel). The p-mode power is rather intermittent on small scales, and is in fact concentrated in intergranular lanes, as shown by Stein & Nordlund (2001). A large scale modulation, correlated with the large scale vertical velocity field, is also discernible. Presumably the large scale modulation is caused by the slightly larger velocity amplitudes present in intergranular lanes inside supergranulation scale downdrafts.

3.2. F-Mode Time-Distance Analysis

An important question is whether local helioseismology methods can recover the flow pattern from the oscillatory component of the surface velocity field in these simulations.

We applied the time-distance technique to the f-mode oscillation, because f-mode is the surface gravity mode and thus contains information about horizontal flows and structures near the surface. Therefore, the time-distance results can be directly compared with the surface properties. The f-mode analysis is commonly used in helioseismology. We isolate the f-mode in k_x, k_y, ν space by retaining only values along a band centered on the theoretical f-mode ridge and setting all other values to zero, and then perform the time-distance analysis, constructing outgoing and ingoing travel time maps, mean travel times and travel time differences. We calculate the horizontal divergence $dV_x/dx + dV_y/dy$ from the simulation data and compare it to the travel time differences map after a low-pass filtering (Fig. 7). As shown by Duvall & Gizon (2000), the travel-time difference is roughly proportional to the horizontal flow divergence. We see a good agreement in the large-scale structures, with

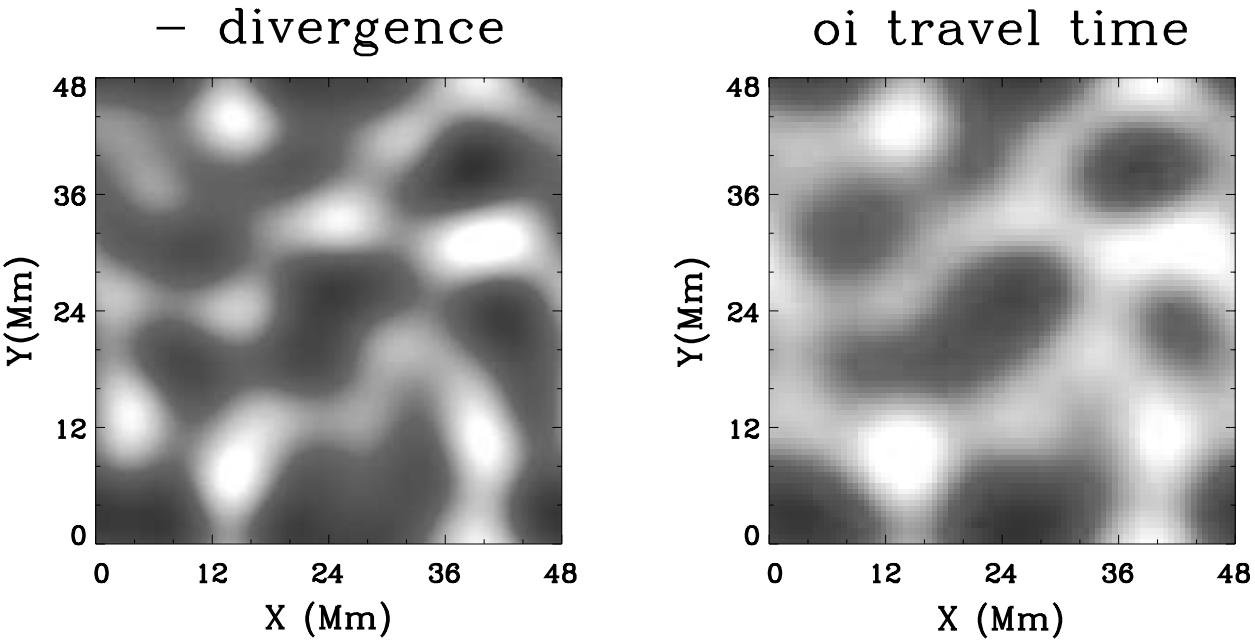

Fig. 7.— Comparison of the simulated horizontal velocity divergence (left; converging flows are light, diverging flows are dark) with f-mode outgoing and ingoing travel time difference map (right; incoming waves are faster in light areas, while outgoing waves are faster in dark areas) after a low-pass filter has been applied. Travel time extrema are 50 s for outgoing and 73 sec for incoming waves.

correlation coefficient 0.88. Calculating east-west and north-south travel time differences, we obtain proxies for horizontal velocity components V_x and V_y. We compare these time difference maps with the actual velocities (Fig. 8). After low-pass filtering, there is a good qualitative agreement between the two, with correlation coefficients 0.7 for x-component and 0.73 for y-component. It is worth mentioning that the time-distance technique measures an

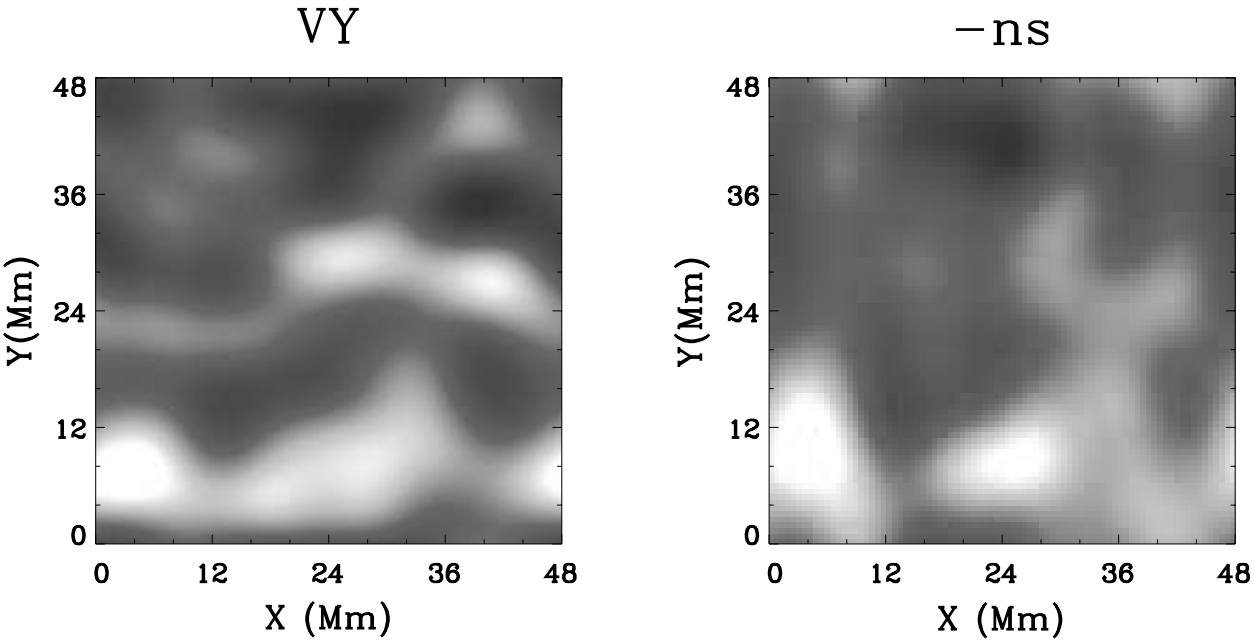

Fig. 8.— Comparison between the simulated horizontal velocity (V_y, left, light is north-bound and dark is south-bound) and f-mode north-south travel time difference map (right, light represents faster north-bound and dark represents faster south-bound waves). A low-pass filtering has been performed here as well. Travel time extrema are 39 s for north-bound and 72 s for south-bound waves.

average over a certain depth, therefore a very high correlation is not to be expected when comparing the time-distance results to a single depth data, particularly above the surface. The agreement might have been better if one looked at a depth representative of the f-mode travel paths, or depth of penetration.

3.3. Local Correlation Tracking

Another possibility for deducing the horizontal velocities is to apply the local correlation tracking (LCT) technique to the vertical velocity. The LCT is a cross-correlation method (e.g. November & Simon 1988) applied to a time series of solar granulation. The cross correlation is spatially localized (within a certain window, usually a Gaussian); its time average presumably measures horizontal displacements of the flows. We apply the LCT technique to the simulated vertical velocity field and compare the resulting horizontal velocity proxies with the simulated horizontal velocity components. Fig. 9 shows the V_y component. Velocities determined by the LCT method are tightly correlated with the simulation velocity, with correlation coefficients

of 0.99 for both V_x and V_y components. However, the LCT amplitudes are a factor 1.8 smaller. Application of a low-pass filter to the simulation velocities brings this ratio down to 1.5. These results are consistent with conclusions of Rieutord et al. (2001). According to them, the horizontal velocity proxies deduced from granular motions underestimate actual velocities by a variable factor, from 2.1 at small scales to 1.6 at large scales.

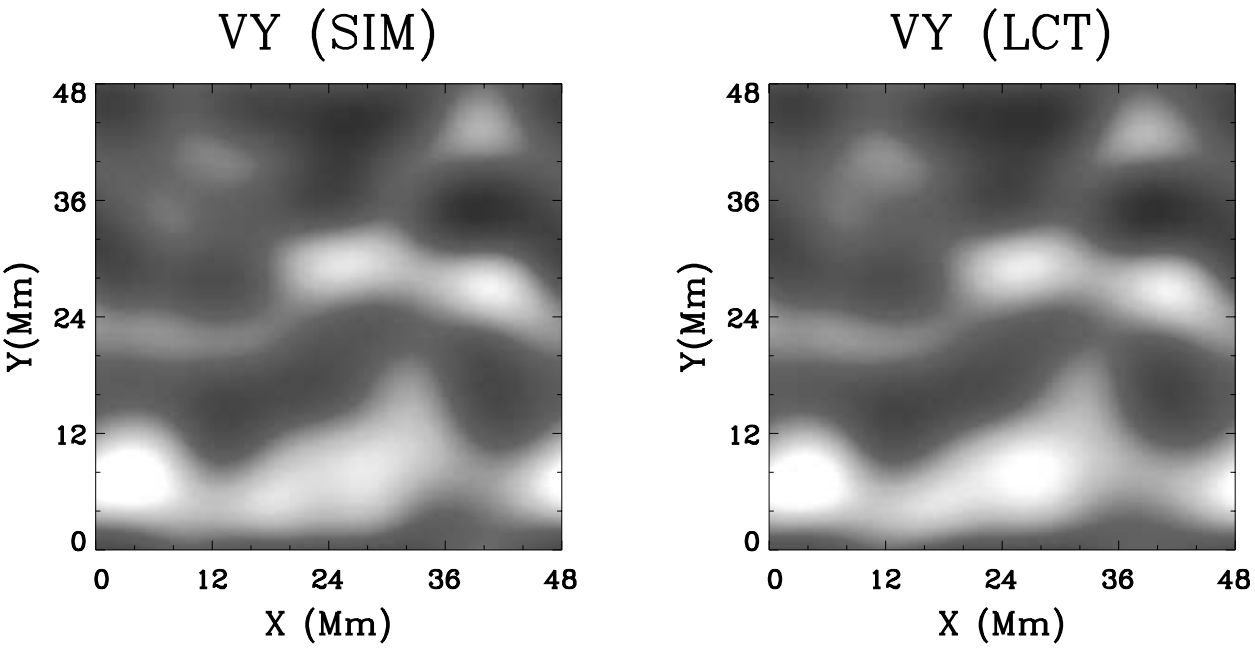

Fig. 9.— Simulated horizontal velocity component V_y (left), averaged over 8.5 hours, and V_y, obtained by LCT analysis (right), after low-pass filtering.

Thus, the realistic simulation data also provide a tool for testing and improving the local correlation tracking techniques.

4. Discussion

The new large-scale realistic 3D radiative-hydrodynamic simulations of the upper layers of solar convection provide an excellent opportunity to validate various techniques, widely used in solar physics and helioseismology for directly obtaining otherwise inaccessible data (subsurface flows and structures, etc). On the other hand, these analysis techniques also help to examine how realistic the simulations are. We have performed an initial analysis of the simulated data and compared our results with the outcome of the SOHO/MDI observations. The similarity between the simulated and observed $\ell - \nu$ and time-distance

diagrams demonstrates that the simulations can be efficiently used to perform and validate local helioseismology techniques. This agreement also reveals a potential for high-resolution time-distance measurements. We carried out f-mode time-distance calculations and local correlation tracking to obtain horizontal velocities. We compare them to the simulated horizontal flows and find a good qualitative agreement. We see large-scale structures in both actual horizontal velocities and their proxies. The results of this investigation provide the basis for further detailed helioseismic analyses of the simulated data, including various scheme of measuring p-mode travel times, approximations for the sensitivity kernels and inversion procedures.

Acknowledgements. DG is grateful for the support of the SOHO/MDI group at Stanford University. DB and RFS were supported by NASA grants NNG04GB92G and NAG 512450 and NSF grants AST-0205500 and AST-0605738. The work of ÅN was supported by a grant from the Danish Natural Science Research Council. Computing time was provided by the Danish Center for Scientific Computing, and by grants from the NASA Advanced Supercomputing Division.

REFERENCES

Benson, D., Stein, R., Nordlund, A. 2006, in H. Uitenbroek, J. Leibacher,, R. F. Stein (eds.), ASP Conf. Ser.: Solar MHD Theory and Observations: a High Spatial Resolution Perspective, 94

Couvidat, S., Birch, A. C., Kosovichev, A. G., Zhao, J. 2004, ApJ, 607, 554

Duvall, T. L., Gizon, L. 2000, Sol. Phys., 192, 177

Duvall, T. L., Jefferies, S. M., Harvey, J. W., Pomerantz, M. A. 1993, Nature, 362, 430

Duvall, T. L., Kosovichev, A. G., Scherrer, P. H., Bogart, R. S., Bush, R. I., de Forest, C., Hoeksema, J. T., Schou, J., Saba, J. L. R., Tarbell, T. D., Title, A. M., Wolfson, C. J., Milford, P. N. 1997, Sol. Phys., 170, 63

Georgobiani, D., Kosovichev, A. G., Nigam, R., Nordlund, Å., Stein, R. F. 2000, ApJ, 530, L139

Gizon, L., Birch, A. C. 2002, ApJ, 571, 966

Jensen, J. M., Duvall, T. L., Jacobsen, B. H., Christensen-Dalsgaard, J. 2001, ApJ, 553, L193

Jensen, J. M., Olsen, K. B., Duvall, Jr., T. L., Jacobsen, B. H. 2003, in H. Sawaya-Lacoste (ed.), ESA SP-517: GONG+ 2002. Local and Global Helioseismology: the Present and Future, p. 319

Kosovichev, A. G., Duvall, T. L. 1997, in ASSL Vol. 225: SCORe'96 : Solar Convection and Oscillations and their Relationship, p. 241

Kosovichev, A. G., Duvall, T. L. . J., Scherrer, P. H. 2000, Sol. Phys., 192, 159

Nordlund, A. 1982, A&A, 107, 1

November, L. J., Simon, G. W. 1988, ApJ, 333, 427

Rieutord, M., Roudier, T., Ludwig, H.-G., Nordlund, Å., Stein, R. 2001, A&A, 377, L14

Scherrer, P. H., Bogart, R. S., Bush, R. I., Hoeksema, J. T., Kosovichev, A. G., Schou, J., Rosenberg, W., Springer, L., Tarbell, T. D., Title, A., Wolfson, C. J., Zayer, I., MDI Engineering Team 1995, Sol. Phys., 162, 129

Sekii, T. 2004, in T. Sakurai, T. Sekii (eds.), ASP Conf. Ser. 325: The Solar-B Mission and the Forefront of Solar Physics, p. 87

Stein, R., Georgobiani, D., Trampedach, R., Ludwig, H.-G., Nordlund, Å. 2004, Sol. Phys., 220, 229

Stein, R. F., Nordlund, Å. 2000, Sol. Phys., 192, 91

Stein, R. F., Nordlund, Å. 2001, ApJ, 546, 585

Werne, J., Birch, A., Julien, K. 2004, in D. Danesy (ed.), ESA SP-559: SOHO 14 Helio- and Asteroseismology: Towards a Golden Future, p. 172

Woodard, M. F., Korzennik, S. G., Rabello-Soares, M. C., Kumar, P., Tarbell, T. D., Acton, S. 2001, ApJ, 548, L103

Zhao, J., Kosovichev, A. G., Duvall, T. L. 2001, ApJ, 557, 384